Biomaterials 103 (2016) 293–304

Contents lists available at ScienceDirect

Biomaterials

journal homepage: www.elsevier.com/locate/biomaterials

Long-term biocompatibility, imaging appearance and tissue effects associated with delivery of a novel radiopaque embolization bead for image-guided therapy

Karun V. Sharma [a], Zainab Bascal [b], Hugh Kilpatrick [b], Koorosh Ashrafi [b], Sean L. Willis [b], Matthew R. Dreher [c], Andrew L. Lewis [b, *]

[a] Children's Hospital, Children's National Medical Center, 1630 Euclid Street NW#1, Washington, DC, USA
[b] Biocompatibles UK Ltd, A BTG International group company, Lakeview, Riverside Way, Watchmoor Park, Camberley, Surrey GU15 3YL, UK
[c] Biocompatibles Inc., A BTG International group company, Five Tower Bridge, Suite 810, 300 Barr Harbor Drive, West Conshohocken, PA 19428, USA

ARTICLE INFO

Article history:
Received 24 March 2016
Received in revised form
27 June 2016
Accepted 29 June 2016
Available online 5 July 2016

Keywords:
Embolization
Radiopaque beads
LC Bead LUMI™
Biocompatibility
X-ray imaging
CT imaging

ABSTRACT

The objective of this study was to undertake a comprehensive long-term biocompatibility and imaging assessment of a new intrinsically radiopaque bead (LC Bead LUMI™) for use in transarterial embolization. The sterilized device and its extracts were subjected to the raft of ISO10993 biocompatibility tests that demonstrated safety with respect to cytotoxicity, mutagenicity, blood contact, irritation, sensitization, systemic toxicity and tissue reaction. Intra-arterial administration was performed in a swine model of hepatic arterial embolization in which 0.22–1 mL of sedimented bead volume was administered to the targeted lobe(s) of the liver. The beads could be visualized during the embolization procedure with fluoroscopy, DSA and single X-ray snapshot imaging modalities. CT imaging was performed before and 1 h after embolization and then again at 7, 14, 30 and 90 days. LC Bead LUMI™ could be clearly visualized in the hepatic arteries with or without administration of IV contrast and appeared more dense than soluble contrast agent. The CT density of the beads did not deteriorate during the 90 day evaluation period. The beads embolized predictably and effectively, resulting in areas devoid of contrast enhancement on CT imaging suggesting ischaemia-induced necrosis nearby the sites of occlusion. Instances of off target embolization were easily detected on imaging and confirmed pathologically. Histopathology revealed a classic foreign body response at 14 days, which resolved over time leading to fibrosis and eventual integration of the beads into the tissue, demonstrating excellent long-term tissue compatibility.

1. Introduction

Embolotherapy is a procedure for introducing a variety of agents into the circulation in order to occlude blood vessels for therapeutic intent, for instance to prevent bleeding, to arrest flow through abnormal connections such as arteriovenous malformations (AVMs) or to devitalise a structure, organ or tumorous mass by inducing ischemic necrosis. Embolic agents come in many different forms including microparticles, pellets, glues or metallic coils [1,2]. These embolics are administered to targeted tissues through a catheter inserted and manoeuvred through the vasculature into the desired location. One common application of this technique is the use of microparticles, most usually microspheres/beads to treat tumors in the liver where the intention is to physically occlude the vessels feeding the tumour in order to induce localised ischemic necrosis of the malignant mass. However, perfect tumour targeting of microparticles is not possible and embolization of normal adjacent healthy liver parenchyma is inevitable. The embolization of healthy liver parenchyma can induce significant local tissue changes, including elevated serum liver enzymes and tissue damage, but these side-effects typically resolve over time [3]. However, there should be no chronic material-related inflammatory reaction or clinical sequelae. The microparticles themselves may disappear over time if bioresorbable, or if non-degradable, should be sufficiently bioinert and well-tolerated in tissue where they reside.

Embolotherpy with microparticles is conducted under X-ray

Abbreviations and acronyms: RO, Radiopaque; TAE, transarterial embolization; CT, computed tomography; DSA, digital subtraction angiography; IV, intravenous; H&E, Hematoxylin and Eosin stain.

* Corresponding author.
E-mail address: andrew.lewis@btgplc.com (A.L. Lewis).

http://dx.doi.org/10.1016/j.biomaterials.2016.06.064

based image guidance where injection of iodine-based liquid contrast agent, a radiodense material, is used to create a roadmap of the network of blood vessels to be embolized. Some embolic devices such as coils are inherently radiopaque which enables them to be easily located during and post procedure. Liquid embolics such as Glue or Onyx® are often mixed with radiodense materials (such as Lipiodol® oil or tantalum powder) prior to use in order to impart radiopacity [4,5]. Microparticles are usually composed of synthetic and natural polymers that are radiolucent and therefore cannot be directly seen during delivery which requires the addition of iodine-based liquid contrast agent to monitor their delivery. However, only the degree of blood flow cessation indicates when sufficient embolic agent has been delivered to achieve the desired flow-based embolization end-point. It has been demonstrated using embolic bead devices that there is a degree of trapped residual soluble contrast agent retention at the site of embolization that dissipates over the next several hours post-procedure [6,7]. CT imaging within a 6 h time frame post-delivery therefore, provides contrast retention as a surrogate marker of bead location and some degree of comfort that the correct blood vessels have been embolized. The exact bead location, however, remains unknown.

The concept of intrinsically radiopaque embolic beads has been explored for many years [8] and multiple experimental studies are available in the literature. In some cases the beads have been made radiodense by the incorporation of metallic components such as tantalum [9] or barium [9,10]. This can have significant effect on the handling and administration of the beads as the increased density induces rapid sedimentation [11]. There is also concern for the long-term fate of the entrapped contrast material and the potential for leaching into the surrounding tissue over time. The incorporation of iodine-containing species into polymers has therefore been a more widely studied approach, resulting in materials useful as bulking agents [12], in bone cements [13,14], for nucleus pulposus replacement [15,16] and as microparticle emboli [17,18]. The radiopacity can be introduced by means of an iodine-bearing monomer at the polymerization stage [17–19] or by chemical attachment of an iodinated species with reactive functionality to preformed polymer microspheres [20]. Compounds based upon iodinated benzyl groups are convenient starting materials for either of these approaches as they provide for synthetic flexibility and enable high iodine content per unit mass. It is for these reasons that such compounds are the basis for most of the commercially-available soluble contrast media (Fig. 1 (1)). Radiopaque beads have been prepared based upon incorporation of 2,3,5 triiodobenzyl moieties (Fig. 1, (3 & 5)) [17], but whilst they possessed high unit iodine content in the 25–30 wt% region, this somewhat compromised the hydrophilicity and softness attributes that are desirable for the handling and microcatheter delivery of embolization beads. Horák et al. tried to address this problem with the synthesis of 3-(methacryloylamido-acetamido)-2,4,6-triiodobenzoic acid (MABA, Fig. 1 (4)) and its subsequent copolymerization with HEMA in the presence of additives to induce porosity to the microspheres [21]. They found it necessary to incorporate at least 27 wt% iodine for adequate radiopacity but they experienced issues with irregular particle formation and agglomeration during the polymerization. Others have attempted to increase the hydrophilicity of the system by utilising the mono-iodinated 2-[4-iodobenzoyl]-oxo-ethyl-methacrylate monomer (4IEMA, Fig. 1, (2)) copolymerised with hydrophilic comonomers such as hydroxyethyl methacrylate (HEMA) or 1-vinyl-2-pyrrolidinone (NVP) [19]. Whilst this did enable the synthesis of some microsphere formulations that were water-swellable in nature, only those with low water content and iodine contents of ~20 wt% were sufficiently radiopaque to be useful in practice.

While it has been difficult to establish a balance between the appropriate physicochemical properties (e.g., water content, density, sphericity, dispersibility) and useful levels of radiopacity, it has been demonstrated that the materials based on the triiodinated chemistry display good biocompatibility [23]. *In vitro* cell-based analyses show no indications of cytotoxicity or effect on cell proliferation, while *in vivo* implantation studies show they are well-tolerated with no signs of adverse tissue reactions. We have therefore recently reported on efforts to modify LC Bead®, well-characterized polyvinylalcohol-based hydrogel beads for embolization of hypervascular tumors and AVMs. Approaches were developed to activate the bead chemistry towards triiodinated species (Fig. 1, (5)) to render them radiopaque whist maintaining their hydrogel nature [20]. We have since optimized this chemistry and have a process for manufacture of intrinsically radiopaque beads (RO Beads) that have water contents in the region of 60–70% with iodine contents in the range 189–258 mg/mL true bead volume (133–177 mg Iodine/mL sedimented beads, equivalent to >60 wt% iodine on a dry mass basis) [22]. This provides for an excellent degree of radiopacity coupled with the benefits of a hydrogel performance (Fig. 1, (scheme 6)). The additional visual information provided by these beads may provide tools for standardization and reproducibility of end points and treatment effects in addition to offering better conspicuity to determine target and non-target embolization [22,24]. Furthermore, the durable imaging appearance of the beads may also aid in the guidance and evaluation of the embolization procedure. Intra-procedural identification of tissue at risk for under-dosing or under-treatment can better inform the physician of options to immediately target this tissue with additional therapies rather than waiting for the outcome of follow-up scans [25]. In this study we present the outcome of the biocompatibility testing of the optimized product, LC Bead LUMI™, and investigate the long-term effects up to 90 days post embolization in a swine liver. We also concurrently examine the bead location with X-ray fluoroscopy and computed tomography (CT) as well as the associated tissue changes resulting as a consequence of their embolization.

2. Materials and methods

2.1. Materials

LC Bead LUMI™ used in this study was prepared and characterized as described previously [22]. Briefly, sulfonate-modified acrylamido-polyvinylalcohol beads were made using a reverse suspension polymerization process [26]. Triiodobenzyl groups were coupled to the PVA chains of the preformed beads using a proprietary process (scheme 6) to yield beads that were sieved into different size fractions, dispensed into vials and steam sterilized. The 70–150 μm size range of RO Beads was selected for the biocompatibility and embolization studies as these provide a high challenge given the large number of beads and high surface area for a given volume. Visipaque™ 320 was used to make the bead suspension. Each vial of beads (2 mL volume was mixed with 18 mL of contrast agent taking care to eliminate any air bubbles from the mixture.

2.2. ISO10993 biocompatibility studies

The biological evaluation of the RO Beads was based upon the principles of ISO 10993-1: Biological evaluation of medical devices-Part 1: Evaluation and testing within a risk management process (ISO 10993-1: 2009). The biological evaluation took into account the anticipated nature and duration of contact with RO Bead, which is a permanent implanted device in contact with blood. All biocompatibility testing studies (*in vitro* and *in vivo*) were

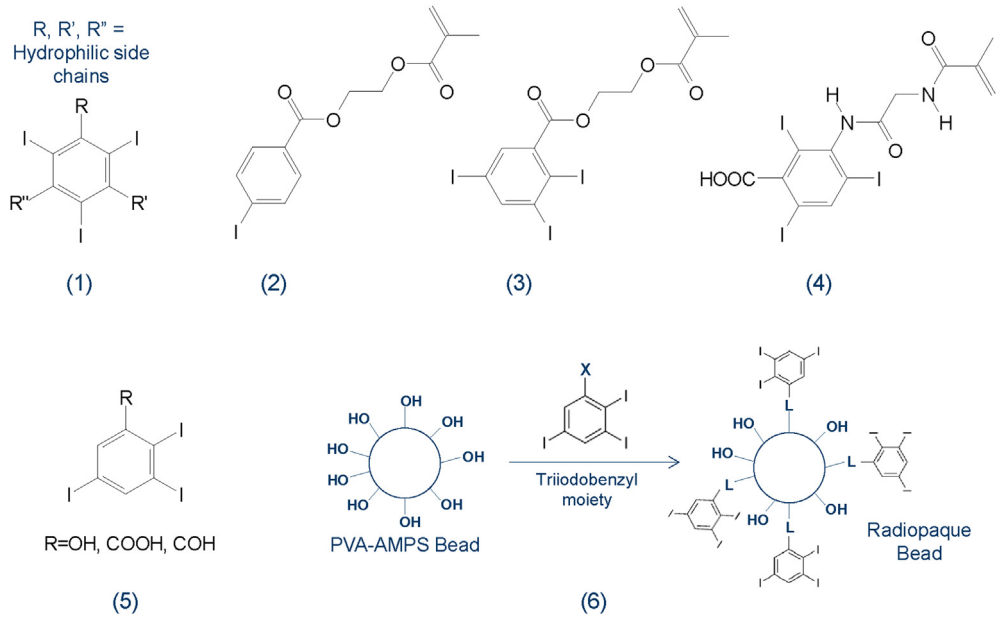

Fig. 1. The 2,4,6 triiodinated benzyl nucleus used in commercial contrast media (1); Examples of Iodinated vinylic monomers used in microsphere synthesis (2–4); Various 2,3,5 triiodinated compounds used to couple to polymers (5); and the schematic process for LC Bead LUMI™ synthesis [22](6).

performed by NAMSA (Northwood, OH, USA) in accordance with current Good laboratory Practice (GLP) regulations. In vivo studies conformed to NAMSA Standard Operating Procedures that are based on the "Guide for the Care and Use of Laboratory Animals, National Academy Press, Washington, D.C., 2011."

2.3. Imaging evaluations in swine liver embolization safety model

2.3.1. Study design

The use of a control group is uncommon in this type of safety assessment and not straight forward where both biocompatibility and imaging aspects are under investigation. The non-radiopaque equivalent of LC Bead LUMI™ is LC Bead™, which has itself been tested in large animal safety studies and hence the biocompatibility and tissue reaction to the bland embolization using this device is known and reported [3]. From an imaging perspective, the usefulness of RO Beads regarding intra-procedural visibility has been demonstrated already using control non-RO and RO Beads without contrast in two recently published articles [22,24]. No control group was therefore selected for comparison in this study.

This evaluation was performed in a swine liver embolization safety model [3,27] at MPI Research Inc. (Mattawan, Michigan, USA) using total of ten male experimentally naïve domestic Yorkshire crossbred swine (farm pigs). The study was split into two phases: a shorter pilot study (n = 4 animals) in which a maximum volume of RO Beads permitted delivery was fixed at ≤ 6 mL and sacrifice was scheduled for 14 days; and a longer term main study (n = 6 animals) in which the volume of RO Beads permitted delivery was raised to ≤ 10 mL and sacrifice was scheduled at 32 days (n = 3) and 91 days (n = 3). The purpose of the pilot study was to determine a volume of liver tissue embolized by a given volume of beads, whilst avoiding off-target embolization in adjacent organs such as the stomach, small bowel, pancreas and spleen before proceeding to the longer term study. Imaging was performed at multiple time points across both studies (Table 1) involving X-ray fluoroscopy, digital subtraction angiography (DSA), single shot X-ray and CT with and without IV contrast injection. MPI Research Inc. Standard Operating Procedures conditions conformed to USDA Animal Welfare Act and "Guide for the Care and Use of Laboratory Animals", Institute of Laboratory Animal Resources, National Academy Press, Washington, D.C., 2011.

Table 1
RO Bead imaging study design.

Time point	Pilot study (≤6 mL RO beads)				Main study (≤10 mL RO beads)					
Animal#	1	2	3	4	5	6	7	8	9	10
Predose	X	X	X	X	X	X	X	X	X	X
1 h postdose	X	X	X	X	X	X	X	X	X	X
24 h postdose	–	X	X	–	–	–	–	–	–	–
Day 7	X	–	–	X	X	X	X	X	X	X
Day 14	X†	X†	X†	X†	–	–	–	–	–	–
Day 30	–	–	–	–	X†	X†	X	X†	X	X
Day 90	–	–	–	–	–	–	X†	–	X†	

X = Imaging performed; – = No imaging performed; † = Scheduled sacrifice day.

2.3.2. Hepatic embolization and X-ray imaging

Vascular access was obtained through femoral artery cut-down and a sheath was placed for stable access. Through this sheath, a combination of a guiding catheter, a 2.7 French microcatheter and a microguidewire was used to select the target hepatic lobe arteries. A consistent angiography and embolization protocol was used during the study. Under fluoroscopic guidance, a guiding catheter was placed at the entrance to the coeliac artery and an angiogram was performed to visualize the branches of the coeliac artery. A microwire and microcatheter combination was then used to select the common hepatic artery, and lobar hepatic arteries supplying approximately 50% of the total liver volume. This lobar selection favored the left lateral or left median liver lobe whenever anatomically feasible (to avoid embolization of the cystic artery). In general, a larger artery size with no extrahepatic branches was preferred and care was taken to avoid any vascular spasm or injury during this step. A pre-embolization angiogram was performed to confirm the catheter tip position, define hepatic artery anatomy and blood flow, and visualize the liver volume to be embolized. With the catheter in position and an appropriate target location

identified, the bead suspension was administered slowly under fluoroscopic guidance taking care to minimize reflux and avoid any extra-hepatic non target embolization. A post-embolization angiogram was also obtained. The fraction of liver area embolized was estimated from the post embolization angiography and DSA images. This was correlated and confirmed on the post embolization CT images, which provided a good approximation of the total volume of liver embolized.

LC Bead LUMI™ was prepared as a 1:10 dilution using iodinated contrast medium (Visipaque™ 320) and delivered through the microcatheter under continuous X-ray fluoroscopic guidance. All angiography and embolization procedures were performed using the GE OEC 9000 elite or GE OEC 9800 C-arm units with the standard GE cardiac software package allowing cine loops at 30 frames per second (fps) as well as digital subtraction angiography (DSA). These C-arms allow for some automatic adjustments but basic fluoroscopy parameters used were peak kilovoltage (kVp) range of 85–95 and current range of 30–150 milliamperes (mA) and dose range between 3.5 and 6.5 $mGym^2$. Fluoroscopy and digital subtraction angiography (DSA) images were obtained before and after embolization to document changes in arterial flow and to visualize the location of the beads in the embolized target. The embolization was performed to clinically relevant angiographic endpoint of fill in Ref. [28] and care was taken to minimize off target embolization. Review and comparison of pre- and post-embolization fluoroscopy and DSA images demonstrated the embolized target lobe(s), associated changes in blood flow, and location of RO Beads in each animal. Single shot X-ray images were also obtained with temporary suspension of respiration (to improve image quality) approximately 5 min after completion of embolization to also allow for "wash out" of residual liquid contrast and better visualize the RO Beads.

2.3.3. CT imaging and analysis

All CT scans were performed using a GE Lightspeed 16 CT scanner and performed with helical acquisition using the following parameters: thickness 1.25 mm, interval 1.25, kV 120, and mA 220–350. Multiplanar reformation in sagittal and coronal planes was also performed. Abdominal CT scans without administration of IV contrast were obtained before and 1 h (±30 min) after embolization with RO Beads. Additional CT scans with and without administration of IV contrast (non-ionic, iso-osmolar IV contrast agent such as Omnipaque™ or Visipaque™ (GE Healthcare)) were obtained at 1, 7, 14, 30 and 90 days following embolization according to the imaging schedule in Table 1. The contrast-enhanced CT images in this study were routinely acquired in both portal-venous and arterial phase (along with non-contrast enhanced CT images). To the experienced user, close inspection of arterial phase CT images does show subtle differences in appearance of arteries containing RO Beads compared to those without beads, but this may not be clinically relevant compared to the non-contrast and portal-venous phase CT images. The non-contrast phase clearly shows the location and distribution of the beads and the portal venous phase shows parenchymal changes and venous structures in addition to the bead-filled arteries. CT Images were reviewed in axial, coronal and sagittal planes as well as in reconstructed maximum intensity projection (MIP) images, by an Interventional Radiologist with over 10 years experience in clinical practice and highly familiar with preclinical evaluation in the porcine liver embolization model. The MIP images display bone and other radiodense structures such as IV contrast and RO bead-filled vessels preferentially with other lower-attenuating structures being less well visualized. The CT scans were reviewed for the following: i) visibility of RO Beads, ii) location RO Beads within the liver, iii) approximate area/volume of liver embolized, iv) extrahepatic off target embolization in adjacent organs including the stomach, duodenum, spleen, pancreas and lungs, v) and other imaging findings which could be related to hepatic embolization and associated ischaemia.

2.4. Clinical pathology

Clinical pathology evaluations were conducted on all animals before and after embolization on days 2, 7, 14, 21, 32, 61, and 91, as applicable. The animals had access to drinking water but were fasted overnight prior to each scheduled sample collection. Blood samples (approximately 4.8–5.8 mL) were collected from the jugular vein. The samples were collected into the appropriate tubes for evaluation of haematology, clinical chemistry and coagulation parameters. On occasion, blood samples were redrawn from animals if the initial samples had clotted. Urine samples were collected using steel pans placed under the cages for at least 16 h.

2.5. Pathological evaluation in swine liver embolization model

Histopathology was conducted on tissues harvested post sacrifice on the scheduled day (Table 1). Necropsy examinations were performed under procedures approved by a veterinary pathologist on all animals.

2.5.1. Macroscopic analysis

The animals were euthanized by sedation with an intramuscular injection of Telazol, followed by an intravenous overdose of sodium pentobarbital solution and exsanguination by transection of the femoral vessels. The animals were examined carefully for external abnormalities including palpable masses. The skin was reflected from a ventral midline incision and any subcutaneous masses were identified and correlated with antemortem findings. The abdominal, thoracic, and cranial cavities were examined for abnormalities. The organs were removed, examined, and, where required, placed in fixative. Special attention was paid to the liver for abnormalities, as well associated vasculature, surrounding tissue, gallbladder, hepatic bile ducts, GI tract, lungs, heart, kidney, spleen, and brain. All tissues were fixed in neutral buffered formalin.

2.5.2. Microscopic analysis

Microscopic examination of fixed hematoxylin and eosin-stained paraffin sections was performed on sampled sections of tissues. For some sections, Russell-Movat Pentachrome stain was used in order to evaluate the presence of collagen and mucin. The slides were examined by a board-certified veterinary pathologist. Photomicrographs of representative lesions seen during the microscopic examination, including those considered to be treatment related, were taken.

3. Results and discussion

3.1. Biocompatibility testing

The biocompatibility tests conducted and their outcomes are listed in Table 2.

All of the *in vitro* and *in vivo* biocompatibility tests performed showed that neither the RO Bead nor any of its extract solutions elicited any response that would be a concern when extrapolating to the target liver cancer patient population.

3.2. Clinical observations

Over the course of the study, animals consumed their daily allotment of food, gained weight in a normal manner and were

Table 2
Biocompatibility studies carried out on LC Bead LUMI™ and its extracts and their outcomes.

ISO standard	Biocompatibility test	Rationale	Product tested[a]	Pass/Fail
ISO10993 Part 3 Tests for genotoxicity, carcinogenicity and reproductive toxicity	Mouse lymphoma study	To evaluate for mutagenic potential	Extracts in DMSO and Serum-free cell culture medium	Pass
			Packing solution	Pass
	Mouse Peripheral blood Micronucleus Study	To evaluate for the potential to produce cytogenetic damage.	Extracts in saline and sesame oil	Pass
			Packing solution	Pass
	Bacterial Reverse Mutation Study	Rapid screening for determination of mutagenic and potential carcinogenic hazards	Extracts in DMSO and saline	Pass
			Packing solution	Pass
ISO10993 Part 4 Selection of tests for interactions with blood	In vitro Hemolysis Study (Modified ASTM-Direct Contact Method)	To determine whether direct contact with the test article would cause *in vitro* red blood cell hemolysis	RO Beads only	Pass
			Extract in CMF-PBS	Pass
			Packing solution	Pass
ISO10993 Part 5 Tests for *in vitro* cytotoxicity	Cytotoxicity Study using the ISO Elution Method	To evaluate the cytotoxicity of a test article extract using *in vitro* mammalian cell culture test	Extract in single strength Minimum Essential Medium	Pass
			Packing solution	Pass
ISO10993 Part 6 Tests for local effects after implantation	ISO Muscle Implantation Study in the Rabbit (2 weeks)	To evaluate the local tissue response, 2 weeks after surgical implantation	RO Beads only	Pass
	ISO Surgical Muscle Implantation in the Rabbit (26 weeks)	To evaluate the local tissue response, 26 weeks after surgical implantation	RO Beads only	Pass
	Sub chronic Toxicity Study in the Rat following Subcutaneous Implantation (13 weeks)	To evaluate the potential systemic toxicity following subcutaneous implantation as well as local irritation or toxicity at the implant sites	RO Beads only	Pass
ISO10993 Part 10 Tests for irritation and skin sensitization	ISO Sensitization Study in the Guinea Pig	To identify the potential for dermal sensitization	Extracts in saline and sesame oil	Pass
	ISO Acute Intracutaneous Reactivity Study in the Rabbit	To evaluate the local dermal irritant effects	Extracts in saline and sesame oil	Pass
ISO10993 Part 11 Tests for systemic toxicity	ISO Acute Systemic Toxicity Study in the Mouse	To evaluate acute systemic toxicity of a test article following a single intravenous or intraperitoneal injection	Extracts in saline (iv) and sesame oil (ip)	Pass
	Pyrogenicity, Rabbit Pyrogen Study, Material Mediated	To evaluate for material mediated pyrogenicity in the rabbit	Extract in saline	Pass

[a] The extraction conditions for most studies were performed at 70 °C for 24 h.

considered to be in good health. All animals survived to the scheduled necropsy interval with the exception of animal number 10. Animal number 10 was found dead during the anaesthetic recovery period following the Day 32 CT imaging (approximately 1 h after completion of CT scan). Off-target embolization of the phrenic artery (Fig. 5, section 3.2) may have caused respiratory issues that contributed to this animal's early expiration. Prior to the Day 32 imaging procedure, animal number 10 was considered to be in good health and was gaining weight normally.

3.2.1. Haematology

There were no RO Bead-related effects among haematology parameters. All mean and individual values were considered within expected ranges for biological and/or procedure-related variation. At 1 h post-embolization there were mild transient decreases in multiple haematology endpoints that were typical of a dilutional effect caused by intravenous fluid administration during the embolization and imaging procedures. These findings included mild decreases in red cell mass; and leukocyte, platelet, reticulocyte, lymphocyte, monocyte, and basophils counts, relative to pretest. By day 2 these findings had resolved and were generally comparable to pretest for the remainder of the study.

3.2.2. Coagulation

There were no effects of RO Bead on coagulation times (i.e., APTT and prothrombin time) at any collection interval, up to and including the Day 91 collection. All individual and mean values were considered within an acceptable range for biologic, procedure and assay-related variation. There was a mild and transient increase in fibrinogen at the Day 2 and 7 collection (+17–46%), relative to pretest values. Increases in fibrinogen were consistent with an inflammatory stimulus, as related to the anticipated liver tissue injury/embolization; these effects had resolved by Day 14. . All other mean and individual values were considered within expected ranges for biological and procedure-related variation.

3.2.3. Clinical chemistry

At the Day 2 collection, there was evidence of hepatocellular injury, including mild increases in aspartate aminotransferase (AST; +192%), alanine aminotransferase (ALT; +73%), sorbitol dehydrogenase (SDH; +74%), and lactate dehydrogenase (LDH; +84%), relative to pretest values. Hepatocellular injury was attributed to hepatic artery embolization with resulting hepatocellular ischemia. These effects were mostly resolved (levels returned to baseline) by the Day 7 collection. These transient elevations in liver enzymes (transaminitis) are also routinely seen in clinical liver embolization procedures.

3.3. Bead handling, delivery and imaging evaluation – fluoroscopy, DSA and single X-ray

RO Bead suspension (1:10 dilution of beads in iodinated contrast medium) was found to be durable and easy to handle [22]. Agitation of the delivery syringe every two to three minutes was

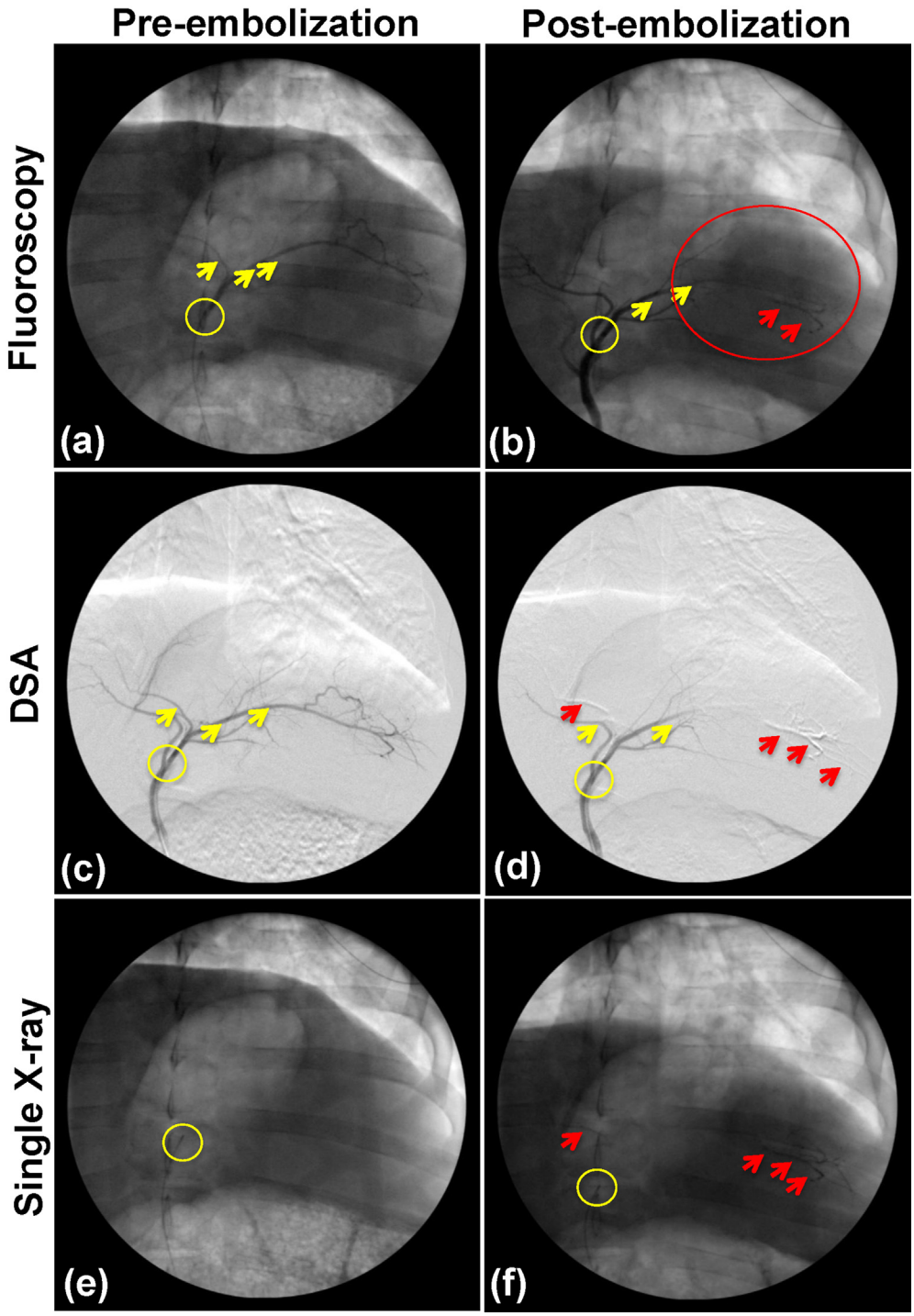

Fig. 2. Fluoroscopic, DSA and single X-ray images pre-embolization (a, c & e respectively) and post embolization (b, d & f respectively). Catheter tip position (yellow circle), embolized left lobe (red circle), embolized arteries (yellow arrows) and RO Beads within target arteries (red arrows) are indicated. Fluoroscopic images (b) were taken during contrast injection and showed the expected alterations in blood flow due to embolization of the left lobe (diversion away from the embolized region) with soluble contrast proximal to the catheter tip with retrograde flow and reflux.

adequate to maintain a good suspension and allowed for effective delivery through the 2.7 French microcatheter without any catheter occlusion. Selective catheterization of the hepatic lobar branches was successfully achieved in all animals (Fig. 2 yellow circle for example) without complication. Embolization was performed using RO Bead suspension volumes ranging from 2.2 to 10 mL (containing 0.22–1.0 mL of 70–150 μm bead volume) across the two phases of the study (Table 3).

Hepatic embolization with RO Beads was performed with careful technique using slow injection and continuous fluoroscopic monitoring to devascularize target arteries (Fig. 2, (b,d) yellow arrows for example) while avoiding reflux and off target extrahepatic embolization. DSA was useful to show hepatic arteries containing RO Beads that no longer filled with IV contrast, demonstrating

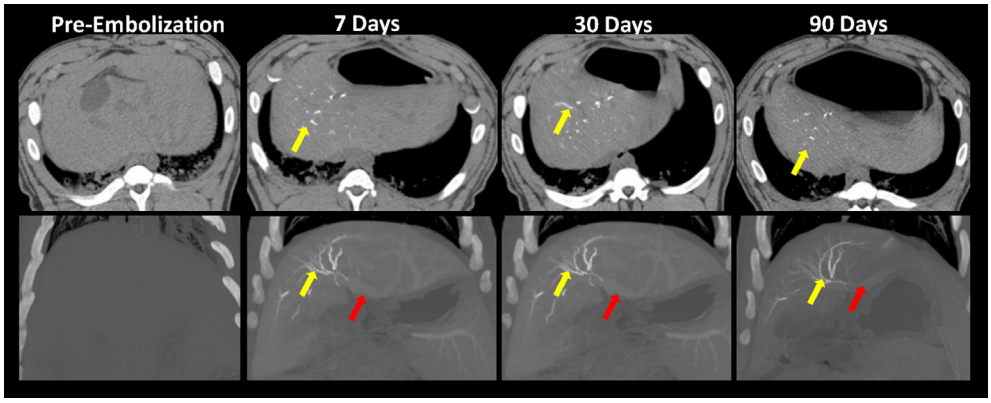

Fig. 3. Durable Visibility of RO Beads Observed with CT Scan. Top row shows images from CT scans obtained without soluble IV contrast (axial plane and soft tissue windows) that clearly demonstrate RO Beads located in hepatic arteries after embolization of swine liver (yellow arrows). CT scans obtained at 7, 30 and 90 days following embolization show the visibility and appearance of RO Beads persists and is unchanged over the 90 days. Bottom row shows images from CT scans obtained with soluble IV contrast (coronal plane and bone windows; maximum intensity projection images) that clearly demonstrate that RO Beads seen in the hepatic arteries (yellow arrows) are more dense than, and clearly differentiated from soluble IV contrast seen that is seen in the portal veins (red arrows).

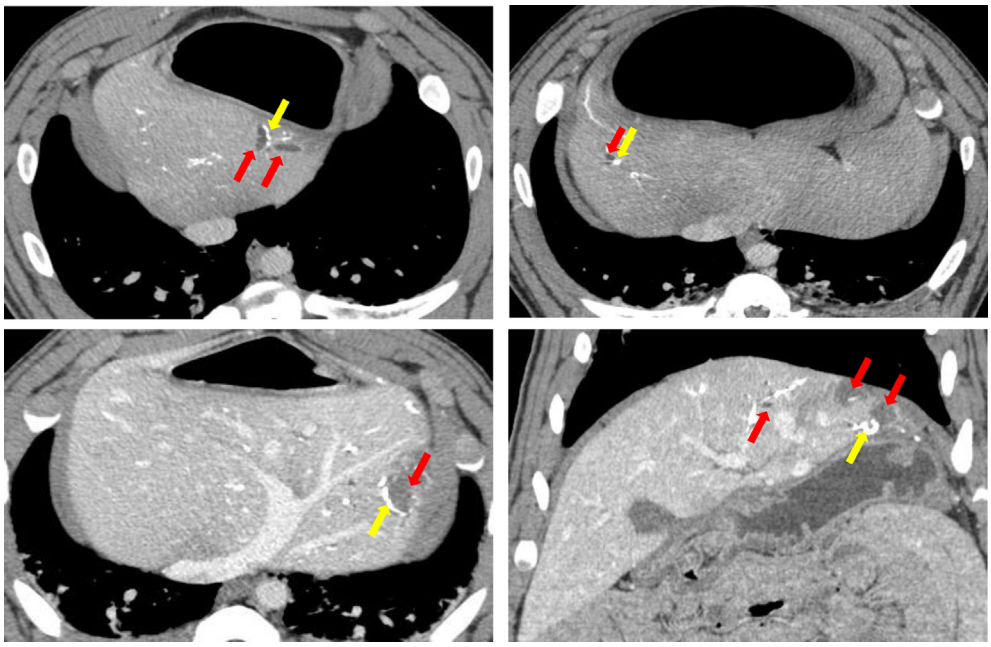

Fig. 4. Tissue Changes Following Swine Liver Embolization. CT scans with soluble IV contrast obtained 30 days following embolization show dilation of bile ducts and small areas of liver ischemia (red arrows) adjacent to hepatic arteries filled with RO Beads (yellow arrows) in two animals. These changes are consistent with ischemia resulting from hepatic arterial embolization.

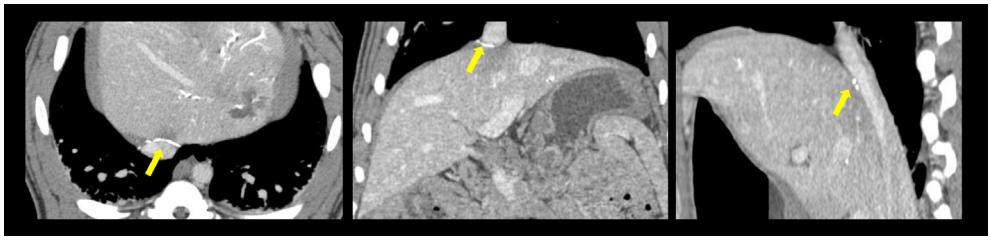

Fig. 5. Non Target Embolization detected with RO Beads. CT scan with soluble IV contrast obtained 30 days following embolization shows RO Beads filling the extrahepatic phrenic artery (yellow arrows) indicating non target extrahepatic embolization which was not noted during embolization.

successful embolization; DSA subtraction artefacts were also indicative of the bead location in the arteries (Fig. 2d). Single shot X-ray (red arrows, Fig. 2f) better visualize RO Beads. It is the case that at very early time points during embolization (seconds to minutes), before soluble contrast washes out, both beads and contrast are present in the arteries and contribute to the observed

Table 3
Embolization procedure details (ND = not determined).

Animal number	Total volume (mL) of RO beads delivered (1:10 dilution)	Extra-hepatic reflux noted during embolization?	Extra-hepatic non-target embolization noted on CT?	Approximate percentage of liver embolized
1	2.2	No	No	ND
2	6.0	No	No	ND
3	5.5	No	No	ND
4	6.0	No	No	ND
5	5.5	No	No	50
6	6.0	No	No	50
7	6.5	No	No	50
8	10	No	No	50
9	7	No	No	50
10	10	No	Yes – phrenic artery	66

image. However, as the soluble contrast washes out, what is seen is largely the contribution of the beads. The CT scans obtained after the procedure and repeated over time up to 90 days (see the following sections) confirm that the areas seen on the fluoroscopy and DSA images were in fact the location of the RO Beads.

3.4. Imaging evaluation – CT imaging analysis

Review of multi-planar CT data sets easily depicted the location and three dimensional distribution of RO Beads within the hepatic arteries of the embolized liver lobes, confirming and further detailing the fluoroscopic findings. Although a systematic and quantitative review of visualized artery size was not undertaken, bead-filled arteries measuring in the range of 1.5–2.5 mm or larger were routinely seen on CT scans. Micro-CT is a higher resolution imaging method that could be used on *ex-vivo* samples to more exquisitely image bead distribution, but it was not performed in this study. We have previously reported on the distributions of similar RO Beads in swine liver using microCT [29]. The correlation between vessel sizes filled with beads and imaged using conventional CT and micro-CT is the subject of a follow-up investigation currently in progress and will be reported separately in due course.

The RO Beads were easily visible on all post embolization CT scans obtained without administration of IV contrast and moreover, was also visible on CT scans obtained after administration of IV contrast (venous phase imaging). This demonstrates that RO Beads are highly dense and can be visualized with CT even in the presence of tissue contrast provided by IV contrast administration (Fig. 3). CT scans obtained over time demonstrate the durable visibility and imaging appearance of RO Beads. Axial plane soft tissue window CT images obtained without soluble contrast administration from a representative animal are shown prior to and then at 7, 30 and 90 days following embolization with RO Beads. These images clearly demonstrate beads located in the hepatic arteries of the embolized swine liver. Clearly, the bright lines of beads are only observed in the post embolization scans and remain visible with no obvious deterioration in image density over the 90 day period of the study. The appearance of the RO Beads in the embolized liver, including their unchanged density and distribution over the 90 day time period are better appreciated on the coronal plane bone window thick slab MIP CT images obtained with soluble contrast administration. These images show bead filled arteries in relation to the soluble contrast filled portal veins.

Close examination of CT scans shows no evidence of off target embolization in adjacent organs including the stomach, duodenum, spleen, pancreas and lungs. In 4 of 10 animals, focal areas of decreased contrast enhancement on venous phase CT images consistent with reduced perfusion and hepatic ischemia in the targeted liver lobes were seen on CT scans obtained 7–90 days after embolization. These expected effects of embolization are shown in Fig. 4. These tissue changes were often closely co-located with the presence arteries densely filled with beads. The overall size of these areas of reduced enhancement often decreased at days 30 and 90 compared to day 7, suggesting some interval recovery. These areas also corresponded to those seen in the pathological analysis composed of wide areas of hepatic necrosis (section 3.4). The 14, 30 and 90 day CT scans also show some dilated bile ducts in the embolized liver, most of which are in a peripheral location (Fig. 4). These are best seen on scans with IV contrast and are often located adjacent to embolized arteries; most likely related to bile duct ischemia caused by embolization. This also correlates well with the observed presence of bile duct hyperplasia seen in some of the pathological analysis of these samples (section 3.4). This is an expected finding as the blood supply to the bile ducts is solely derived from branches of the hepatic artery (which has been embolized). The surrounding hepatocytes, on the other hand, derive their blood supply from both the hepatic artery and portal vein and, therefore are relatively protected from arterial embolization.

Although no off-target embolization to organs adjacent to the liver was seen in any of the animals, one animal (animal 10) failed to reach its scheduled sacrifice time point at 91 days since it did not recover from the anesthesia following the 30 day CT scan. Embolization of the phrenic artery (the blood supply to the diaphragm) was clearly identified by the presence of RO Beads in this artery on the post-embolization CT scans (discovered after necropsy and not specifically examined during the pathology evaluation, Fig. 5). It is possible that the hepatic ischemia/necrosis in the left lobe (possibly a result of the greater volume of liver embolized (66% compared to 50% for the other animals, Table 3) in this animal) and the non-target embolization of the phrenic artery both contributed to difficulty in recovery from anesthesia and early expiration of this animal.

3.5. Pathological evaluation

3.5.1. Macroscopic observations

Macroscopic observations in the embolized portion of the liver included the appearance of multiple focal tan regions. These macroscopic observations were associated with microscopic findings of hepatic necrosis, fibrosis, and leukocyte infiltrates anticipated following embolization of liver arteries with microparticles. In one animal (animal 1), abdominal cavity adhesions (omentum adhered to the gallbladder and right median liver lobe) and swollen/thickened gallbladder were associated with microscopic findings of gallbladder necrosis, oedema, fibrosis, and neutrophil infiltrate due to injection of RO Beads. Review of the imaging confirmed that the artery supplying the gall bladder (cystic artery) was included in the target region embolized in this animal. Therefore, the macroscopic and histological changes observed in the gall bladder were related to and expected from embolization of

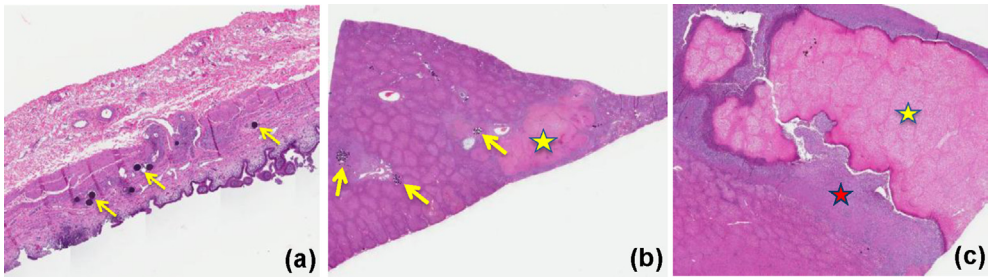

Fig. 6. H&E stained sections of (a) RO Beads in the gallbladder of animal 1 (yellow arrows); (b) areas of focal coagulative necrosis and fibrosis (yellow star) and the presence of clusters of RO Beads (yellow arrows) in animal 3; (c) magnified view of the left lateral lobe of animal 4 showing focal coagulative necrosis (yellow star) and fibrosis (red star).

this artery. No bead-associated tissue changes were present in brain, common bile duct, heart, kidneys, lung, pancreas, spleen, duodenum, jejunum, ileum, and cecum of any of the animals.

3.5.2. Microscopic observations – day 14

RO Beads were present within arteries of the treated liver lobe from all treated animals as expected. In animal number 1 and 3, RO Beads were present within blood vessels of the treated liver lobe and gallbladder (Fig. 6 (a)). Lesions in the gallbladder wall of animal 3 were severe necrosis and oedema, moderate fibrosis, and mild neutrophilic infiltration, which was noted in the CT imaging analysis as abnormal gallbladder wall thickening. Focal coagulative necrosis of several liver lobules and mild increased interlobular fibrosis were present in the treated liver lobes (Fig. 6 (b & c)). These changes are consistent with hepatic ischemia resulting from embolization and also consistent with the areas of decreased enhancement on the CT scans (Fig. 6). In animal number 4 RO Beads were present within blood vessels of treated (left median lobe) and left lateral liver lobes. Focal coagulative necrosis of several liver acini was present in the left lateral liver lobe. A zone of fibrosis and mixed leukocyte infiltrate (primarily neutrophils) was adjacent to the necrotic area (Fig. 6 (c)).

RO Beads were often observed clustered together within the larger arteries (Fig. 7). The beads appear as dark blue objects due to the H&E staining and maintain a spherical morphology in the vessels, surrounded in a matrix of granulation tissue. Often the bead may appear misplaced out of the artery, or completely missing, leaving a hole where it was originally embedded; this is an artefact of the sectioning of the sample (Fig. 7 (b)). Enlarged bile ducts are also visible, a hyperplasia associated with the ischemia induced by the embolization of the artery which provides the bile duct blood supply. This observation supports the presence of dilated bile ducts noted on the CT imaging shown in Fig. 4.

3.5.3. Microscopic observations – day 32

Occlusion of medium sized arteries (typically 0.5–1 mm in diameter) was noted in animals 6 and 10 (Fig. 8). Affected arteries had lodged beads surrounded by mesenchymal/epithelial cells and deposition of mucin and connective tissue resulting in complete filling (occlusion) of the vessel lumen. The beads took on an interesting pattern of staining from the Pentachrome stain used to highlight the connective tissues, appearing like frogspawn with a clear outer layer (Fig. 8(c&d)). The endothelium of affected vessels was frequently absent and the beads were immediately adjacent to the elastic membrane. Microvascular networks (neovascularization) were present within the newly formed intravascular connective tissue stroma in some sections. These tissue observations are consistent with a the classic foreign body response, with the arterial structure being remodelled with an initial invasion of inflammatory cells with these subsequently replaced by connective tissues with the beads being walled off by a fibrotic layer (Fig. 8(c&d)).

3.5.4. Microscopic observations – day 91

On Day 91, RO Beads were present in remnants of blood vessels or what appeared to be hepatic parenchyma. In arteries, the lumens were replaced by mature-appearing collagen/connective tissue that occluded the vessel and encompassed the beads. Small arteries/

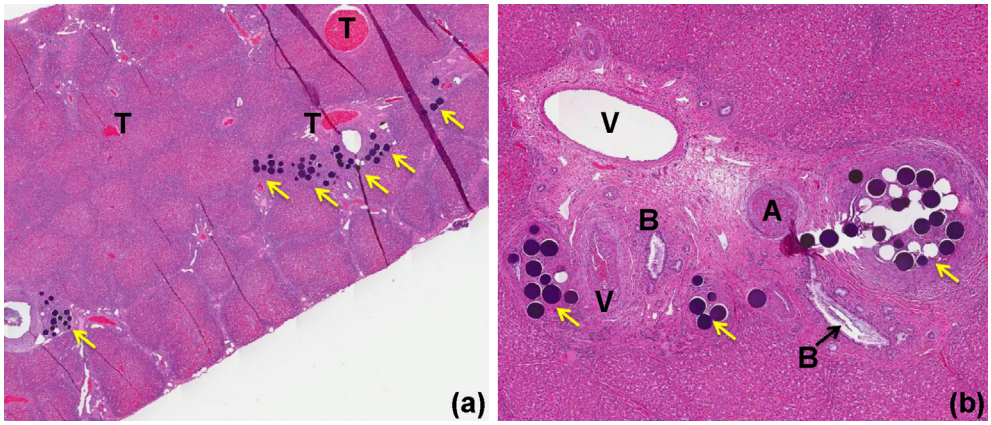

Fig. 7. H&E sections from animal 2, day 14: (a) RO Beads were present within arteries of the treated liver lobe (yellow arrows). Minimally increased interlobular fibrosis was present around liver lobules. Thrombus was often present in small blood vessels (T); (b) RO Beads inside the hepatic artery branch located in a classic triad of artery (A), portal vein (V) and bile duct (B). The black arrow denotes an enlarged bile duct close to an embolized artery. Thrombus is also present in a branch of the artery A.

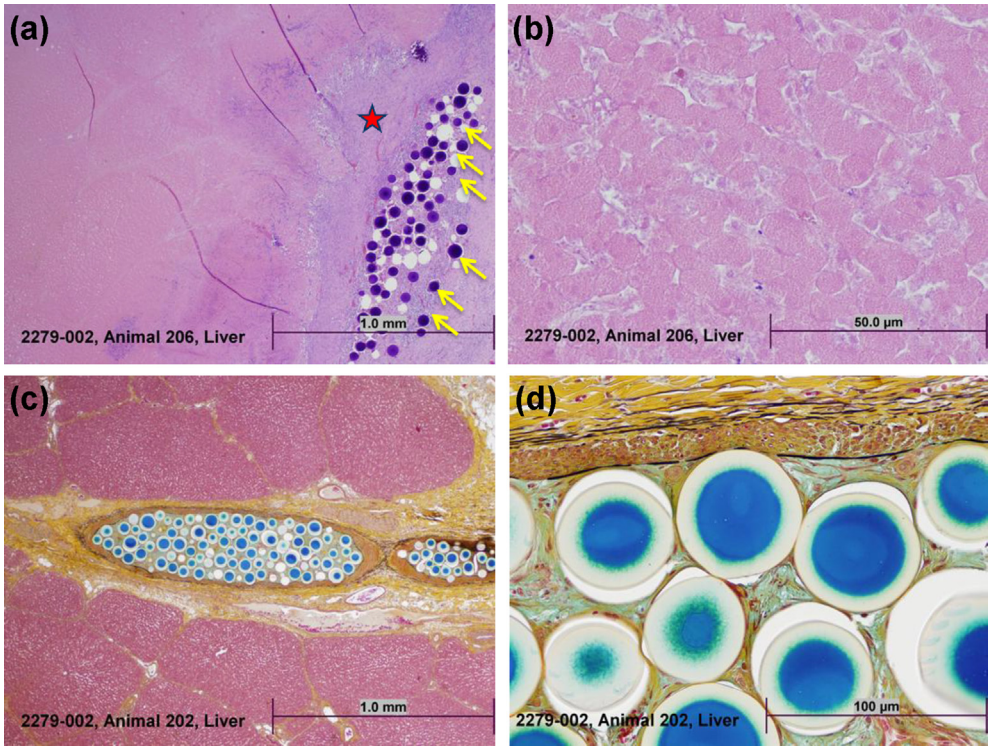

Fig. 8. Stained sections of the liver, Day 32. H&E stain, animal 10: (a) Clusters of RO Beads are visible in a large artery, surrounded by an area of hepatocyte necrosis, fibrosis and inflammation encapsulating the necrosis (red star); (b) High magnification of the coagulative necrosis of hepatocytes-note the absence of cell in this tissue matrix. Pentachrome stain, animal 6: (c) Cluster of beads in medium size artery stained using Russell-Movat Pentachrome stain revealing a collagen-rich layer surrounding the beads (yellow); (d) Higher magnification of RO Beads within the lumen of a medium sized artery (Russell-Movat Pentachrome stain, Collagen: Yellow; Elastic Fibres: Black to Blue/Black; Mucin: Blue).

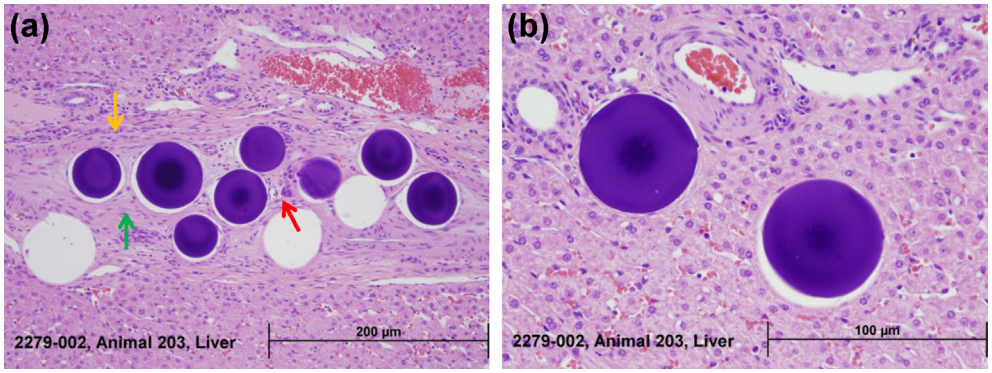

Fig. 9. H&E sections of liver, Day 91. (a) Lumen of an artery in the liver containing beads surrounded by mature collagen filling the space between beads. Clear spaces are presumed to be sites of beads that were displaced during tissue processing. Small arteries/veins were present in the new intravascular connective tissue stroma (red arrow, neovascularization; green arrow, mature collagen; yellow arrow, tunica muscularis of artery wall). (Hematoxylin-Eosin stain); (b) Beads within the parenchyma of the liver without evidence of a tissue injury or inflammatory response. Classic triad of artery (A), vein (V) and bile duct (B). (Hematoxylin-Eosin stain).

veins were present in the new collagen/connective tissue (Fig. 9). Individual beads were observed interspersed between hepatocytes. The beads were frequently near blood vessels but were surrounded by hepatocytes. There was no evidence of tissue injury or inflammatory response to the beads indicating that the material that the beads are composed of is highly biocompatible in nature.

4. Conclusions

The objective of this study was to evaluate the safety, biocompatibility, imaging appearance and tissue effects of hepatic embolization with a novel radiopaque bead (an embolic agent, 70–150 µm in size), in a swine model. The results of this study demonstrate that administration of up to 1 mL of sedimented LC Bead LUMI™ *via* the hepatic artery produced no effect on food consumption and the ability to gain body weight, electrocardiographic endpoints and urinalysis parameters. Transient changes were noted in haematology and coagulation values but these were considered to be related to the embolization-associated ischaemia. Embolization with RO Beads was also associated with minimal transient increases in the activities of AST and ALT on Day 2, but these had resolved by Day 7 as previously observed in this model [3]. These findings are typical of clinical ischemic hepatocellular injury and were anticipated as a result of acute hypoxia induced in

liver tissue by the embolization.

LC Bead LUMI™ in this study is shown to be highly biocompatible, having passed all standard ISO10993 biocompatibility tests. Histopathological analysis of the device at 14, 30 and 90 days showed a classic foreign body response with initial inflammation, fibrosis and tissue remodelling to yield complete integration of the device into the tissue with no observed chronic inflammatory response. This study also demonstrates that this device performs its intended primary function of being able to embolize arteries, leading to targeted regions of ischemia and induction of focal areas of tissue necrosis located adjacent to the beads. Features such as dilated bile ducts or gallbladder embolization were expected as a consequence of the embolization procedure, were noted in the histopathology and correlated well with features observed during the CT imaging analysis. The lack of any loss of RO Bead image intensity over the 90 day period and the completely benign response to the tissue surrounding the beads suggests no loss of the triiodinated species over this time frame *in vivo*, confirming that the covalent attachment of the radiopaque moiety to the bead is stable in the body.

A useful aspect of this novel device is its inherent radiopacity, allowing it to be visualized on X-ray angiography during the embolization procedure, enabling the user to observe filling of target arteries and also potentially off-target arteries if reflux occurs or the catheter is misplaced [22,25]. It should be noted that it is currently recommended that LC Bead LUMI™ is administered as a suspension in pure iodinated liquid contrast medium in order to (i) better suspend the beads and (ii) allow a sense of directionality and flow velocity when injecting very small aliquots of suspension. As both the beads and contrast agent are radiopaque by virtue of the presence of iodine in their structures, they cannot be distinguished from one-another with fluoroscopy as they leave and flow away at the microcatheter tip. Once trapped in the artery, beads become more distinguishable as the liquid contrast medium washes away (the majority in minutes but a small residual amount can be trapped for some hours if the degree of embolization is high). As small vessels well below 0.4 mm in diameter can be clearly seen under single shot resolution [22] then the initiation of non-target embolization may be observed early on and action taken to avoid additional off-target vessel occlusion. In some cases this early signal may be sufficient to avoid significant damage but this will be highly dependent upon the criticality of the non-target vessels embolized. Indeed, in this study a contributory cause of the early expiration of one of the animals was off-target embolization of the phrenic artery, which even though could be clearly seen on the 30 day CT images, was not recognized at the time of the procedure.

In addition to X-ray, the RO Beads are also clearly visible on CT, a finding shown on the 7, 14, 30 and 90 day CT scans obtained with or without IV contrast administration as the beads are more radiodense than the IV contrast and appear brighter. The beads are best seen without IV contrast, as they are easily visible in branches of the hepatic arteries without the confounding influence of soluble contrast in the tissue and the CT imaging appearance remains consistent over the 90 day study period. This will allow the physician to know the exact position of the beads on CT scans performed shortly after embolization and on long-term follow-up CT scans which along with MRI (magnetic resonance imaging) are routinely used in clinical practice to follow progress of liver cancer patients that have been treated with transarterial embolotherapy. It is hoped that the ability to clearly identify the location of the beads during and post-delivery will enable the interventional radiologist performing embolotherapy to better identify areas of undertreatment and be more wary of potential off-target occurrences. LC Bead LUMI™ therefore represents a true step forward in the improvement of minimally-invasive image-guided transarterial embolization.

Acknowledgements

Thanks to MPI Research Inc. (Mattawan, Michigan, USA) for conducting the swine safety studies and to NAMSA (Northwood, OH, USA) for conducting the *in vitro* and *in vivo* biocompatibility studies. All studies were funded by Biocompatibles UK Ltd., a BTG International group company. All co-authors other than KVS are employees of Biocompatibles UK Ltd or Inc.

References

[1] R. Loffroy, B. Guiu, J.P. Cercueil, D. Krause, Endovascular therapeutic embolisation: an overview of occluding agents and their effects on embolised tissues, Curr. Vasc. Pharmacol. 7 (2009) 250–263.
[2] S. Vaidya, K.R. Tozer, J. Chen, An overview of embolic agents, Semin. Interv. Radiol. 25 (2008) 204–215.
[3] A.L. Lewis, R.R. Taylor, B. Hall, M.V. Gonzalez, S.L. Willis, P.W. Stratford, Pharmacokinetic and safety study of doxorubicin-eluting beads in a porcine model of hepatic arterial embolization, J. Vasc. Interv. Radiol. 17 (2006) 1335–1343.
[4] J. Papo, M. Baratz, E. Merimsky, Infarction of renal tumors using isobutyl-2 cyanoacrylate and lipiodol, Am. J. Roentgenol. 137 (1981) 781–785.
[5] A. Komemushi, N. Tanigawa, Y. Okuda, H. Kojima, H. Fujii, Y. Shomura, et al., A new liquid embolic material for liver tumors, Acta Radiol. 43 (2002) 186–191.
[6] Y.S. Golowa, J. Cynamon, J.F. Reinus, M. Kinkhabwala, M. Abrams, M. Jagust, et al., Value of noncontrast CT immediately after transarterial chemoembolization of hepatocellular carcinoma with drug-eluting beads, J. Vasc. Interv. Radiol. 23 (2012) 1031–1035.
[7] J. Suk Oh, H. Jong Chun, B. Gil Choi, H. Giu Lee, Transarterial chemoembolization with drug-eluting beads in hepatocellular carcinoma: usefulness of contrast saturation features on cone-beam computed tomography imaging for predicting short-term tumor response, J. Vasc. Interv. Radiol. 24 (2013) 483–489.
[8] B.C. Thanoo, A. Jayakrishnan, Radiopaque hydrogel microspheres, J. Microencapsul. 6 (1989) 233–244.
[9] B.C. Thanoo, A. Jayakrishnan, Tantalum loaded silicone microspheres as particulate emboli, J. Microencapsul. 8 (1991) 95–101.
[10] U. Stampfl, C.M. Sommer, N. Bellemann, M. Holzschuh, A. Kueller, J. Bluemmel, et al., Multimodal visibility of a modified polyzene-F-coated spherical embolic agent for liver embolization: feasibility study in a porcine model, J. Vasc. Interv. Radiol. 23 (2012), 1225–1231 e2.
[11] L.S. Peixoto, P.A. Melo, M. Nele, J.C. Pinto, Expanded core/shell poly(vinyl acetate)/poly(vinyl alcohol) particles for embolization, Macromol. Mater. Eng. 294 (2009) 463–471.
[12] K. Saralidze, Y.B. Aldenhoff, M.L. Knetsch, L.H. Koole, Injectable polymeric microspheres with X-ray visibility. Preparation, properties, and potential utility as new traceable bulking agents, Biomacromolecules 4 (2003) 793–798.
[13] E.J. Boelen, G. Lewis, J. Xu, T. Slots, L.H. Koole, C.S. van Hooy-Corstjens, Evaluation of a highly-radiopaque iodine-containing acrylic bone cement for use in augmentation of vertebral compression fractures, J. Biomed. Mater. Res. Part A 86 (2008) 76–88.
[14] C.S. van Hooy-Corstjens, S.K. Bulstra, M.L. Knetsch, P. Geusens, R. Kuijer, L.H. Koole, Biocompatibility of a new radiopaque iodine-containing acrylic bone cement, J. Biomed. Mater. Res. B Appl. Biomater. 80 (2007) 339–344.
[15] E.J. Boelen, L.H. Koole, L.W. van Rhijn, C.S. van Hooy-Corstjens, Towards a functional radiopaque hydrogel for nucleus pulposus replacement, J. Biomed. Mater. Res. B Appl. Biomater. 83 (2007) 440–450.
[16] E.J. Boelen, C.S. van Hooy-Corstjens, S.K. Bulstra, A. van Ooij, L.W. van Rhijn, L.H. Koole, Intrinsically radiopaque hydrogels for nucleus pulposus replacement, Biomaterials 26 (2005) 6674–6683.
[17] D. Horak, M. Metalova, F. Svec, J. Drobnik, J. Kalal, M. Borovicka, et al., Hydrogels in endovascular embolization. III. Radiopaque spherical particles, their preparation and properties, Biomaterials 8 (1987) 142–145.
[18] D. Horak, F. Svec, J. Kalal, A. Adamyan, N. Skuba, M. Titova, et al., Hydrogels in endovascular embolization. IV. Effect of radiopaque spherical particles on the living tissue, Biomaterials 9 (1988) 367–371.
[19] C.S. van Hooy-Corstjens, K. Saralidze, M.L. Knetsch, P.J. Emans, M.W. de Haan, P.C. Magusin, et al., New intrinsically radiopaque hydrophilic microspheres for embolization: synthesis and characterization, Biomacromolecules 9 (2008) 84–90.
[20] A.H. Negussie, M.R. Dreher, C. Gacchina Johnson, Y. Tang, A.L. Lewis, G. Storm, et al., Synthesis and characterization of image-able polyvinyl alcohol microspheres for chemoembolization and X-ray-based imaging, J. Mater. Sci. Mater. Med. 26 (2015) 5530–5533.
[21] D. Horak, M. Metalova, F. Rypacek, New radiopaque polyHEMA-based hydrogel particles, J. Biomed. Mater. Res. 34 (1997) 183–188.
[22] R. Duran, K. Ashrafi, K.V. Sharma, M.R. Dreher, S. Mirpour, M. Lin, et al., A novel inherently radiopaque bead for intra-procedural monitoring and post-procedural evaluation of embolization to treat liver cancer, Theranostics

6 (2016) 28–39.
[23] P.J. Emans, K. Saralidze, M.L. Knetsch, M.J. Gijbels, R. Kuijer, L.H. Koole, Development of new injectable bulking agents: biocompatibility of radiopaque polymeric microspheres studied in a mouse model, J. Biomed. Mater. Res. Part A 73 (2005) 430–436.
[24] V. Tacher, R. Duran, L. MingDe, J.H. Sohn, K.V. Sharma, Z. Wang, et al., Multimodality imaging of lipiodol-loaded radiopaque microspheres in transarterial embolization of rabbits with VX2 liver tumors, Radiology 279 (2016) 741–753.
[25] E.B. Levy, V.P. Krishnasamy, A.L. Lewis, S. Willis, C. Macfarlane, V. Anderson, et al., First human experience with directly image-able iodinated embolization microbeads, Cardiovasc. Interv. Radiol. 39 (2016) 1177–1186.
[26] A.L. Lewis, M.V. Gonzalez, S.W. Leppard, J.E. Brown, P.W. Stratford, G.J. Phillips, et al., Doxorubicin eluting beads - 1: effects of drug loading on bead characteristics and drug distribution, J. Mater. Sci. Mater. Med. 18 (2007) 1691–1699.
[27] A.L. Lewis, R.R. Holden, S.T. Chung, P. Czuczman, T. Kuchel, J. Finnie, et al., Feasibility, safety and pharmacokinetic study of hepatic administration of drug-eluting beads loaded with irinotecan (DEBIRI) followed by intravenous administration of irinotecan in a porcine model, J. Mater. Sci. Mater. Med. 24 (2013) 115–127.
[28] R. Lencioni, T. de Baere, M. Burrel, J.G. Caridi, J. Lammer, K. Malagari, et al., Transcatheter treatment of hepatocellular carcinoma with doxorubicin-loaded DC bead (DEBDOX): technical recommendations, Cardiovasc. Interv. Radiol. 35 (2012) 980–985.
[29] K.V. Sharma, M.R. Dreher, Y. Tang, W. Pritchard, O.A. Chiesa, J. Karanian, et al., Development of “imageable” beads for transcatheter embolotherapy, J. Vasc. Interv. Radiol. 21 (2010) 865–876.